Topology and the Kardar-Parisi-Zhang universality class

Silvia N. Santalla[1,5,][*] Javier Rodríguez-Laguna[2,5], Alessio Celi[3], and Rodolfo Cuerno[4,5]

[1]*Departamento de Física, Universidad Carlos III de Madrid, Spain*
[2]*Departamento de Física Fundamental, Universidad Nacional de Educación a Distancia (UNED), Spain*
[3]*Institute of Photonic Sciences (ICFO), Barcelona, Spain*
[4]*Departamento de Matemáticas, Universidad Carlos III de Madrid, Spain*
[5]*Grupo Interdisciplinar de Sistemas Complejos (GISC)*

We study the role of the topology of the background space on the one-dimensional Kardar-Parisi-Zhang (KPZ) universality class. To do so, we study the growth of balls on disordered 2D manifolds with random Riemannian metrics, generated by introducing random perturbations to a base manifold. As base manifolds we consider cones of different aperture angles θ, including the limiting cases of a cylinder ($\theta = 0$, which corresponds to an interface with periodic boundary conditions) and a plane ($\theta = \pi/2$, which corresponds to an interface with circular geometry). We obtain that in the former case the radial fluctuations of the ball boundaries follow the Tracy-Widom (TW) distribution of the largest eigenvalue of random matrices in the Gaussian orthogonal ensemble (TW-GOE), while on cones with any aperture angle $\theta \neq 0$ fluctuations correspond to the TW-GUE distribution related with the Gaussian unitary ensemble. We provide a topological argument to justify the relevance of TW-GUE statistics for cones, and state a conjecture which relates the KPZ universality subclass with the background topology.

PACS numbers: 68.35.Ct, 02.40.-k, 64.60.Ht, 61.43.Hv

I. INTRODUCTION

Growth is about geometry, even in the presence of noise. The Kardar-Parisi-Zhang (KPZ) universality class, which describes the fluctuations of growing interfaces, [1, 2] is known to also describe the statistics of the boundaries of balls with increasing radii on random manifolds which are flat on average [3]. Remarkably, for one-dimensional interfaces evolving in two-dimensional space, the KPZ class does not only entail the values of the critical exponents, but also the full probability distribution for the one-point and the two-point fluctuations, which were initially conjectured and later shown to follow Airy processes [4–7], see e.g. [8] for a recent review. Nonetheless, at this level the class splits into different subclasses, as occurs when considering for instance growth geometries frequently found in experiments and many continuum and discrete model systems. For instance, in band geometry, i.e., for an interface with periodic boundaries, the local fluctuations are ruled by the Tracy-Widom distribution for the largest eigenvalue of random matrices in the Gaussian orthogonal ensemble (TW-GOE) [9–11]. However, if the interface has an overall circular shape, the fluctuations are those characteristic of the Gaussian unitary ensemble (TW-GUE). What is the origin of such a splitting of the class into two topological flavors? Recent work on discrete growth models and the KPZ equation itself [12, 13] shows that, if the interface is in a band geometry but the underlying substrate is growing, the fluctuations are TW-GUE, just as in the circular case. This shows that the interface does not need to have a non-zero

global curvature for TW-GUE statistics to occur.

All these considerations point to relevant questions: what kind of change takes place in the KPZ subclass when the topology of the base manifold on which growth takes place is changed? What are the relevant subclasses occurring? The possibility of exploring the KPZ class on any Riemannian manifold was already put forward with the proposal of a *covariant form* of the KPZ equation, which was used to explore band and circular geometries simply by changing the base manifold [14, 15]. It was shown that, before reaching the KPZ behavior, the system explored a transient state: an Edwards-Wilkinson (EW) or a self-avoiding walk (SAW) crossover for band and circular geometry, respectively. As a particular case, in the absence of noise or diffusive terms one can study the equation which merely propagates an interface with a constant speed along the local normal direction —related with the level set equation in the case of the dynamics of function graphs [16]—, which we call *Huygens equation*. If applied to an infinitesimal circle, such an equation yields balls of increasing radii around the central point. In [3], such a Huygens equation was studied on random or disordered Riemannian manifolds with short-range correlations, which are flat on average. The dynamics of ball boundaries with increasing radii were shown to fall into the KPZ universality class, the radial fluctuations following the TW-GUE distribution. A relevant point is that transients were absent in this case: KPZ universal behavior was reached already for very short times.

In this work we study the effect of topology on the subclass structure of the KPZ universality class of one-dimensional interfaces, by exploring the interface fluctuations for growing balls on different types of random Riemannian manifolds. More concretely, we study the interfaces developed by the Huygens equation on cones

---

[*] silvia.santalla@uc3m.es

1

of different opening angles, including the limiting cases of the cylinder and the plane, which is the case studied in [3]. See Fig. 1 for an illustration.

Our overall conclusion is that TW-GOE statistics are characteristic of the cylinder, TW-GUE behavior occurring for cones of arbitrary aperture angles θ, including the plane ($\theta = \pi/2$). Hence, a change takes place in the KPZ universality subclass between TW-GUE and TW-GOE as the aperture angle of the base cone manifold is changed, for $\theta = 0$. Transitions among the various KPZ subclasses have been previously explored, although mostly when considering particular initial conditions which are such that, at long times, the interface divides into spatial regions in which statistics are of one or the other subclass. See e.g. [17] for the case of the totally asymmetric simple exclusion process (TASEP) model with an initial condition where particles are placed at the negative even integers. Or the KPZ equation with a double-wedge initial condition or, equivalently, a directed polymer with an end-point which is fixed and the other one is on a half-line [18]. In our present case, the statistics are homogeneous throughout the system and change abruptly from TW-GOE to TW-GUE as soon as the aperture angle is non-zero. Such a result complements those obtained in growing systems with a band geometry [12, 13], in the sense that these two are the only relevant subclasses in the presence of this type of topological changes.

This paper is structured as follows. Section II discusses our general framework: the covariant KPZ equation and Huygens equation, considered on random conformal deformations of a given base manifold. In section III we describe the parametrization that we will use for the cylinder, cones and plane, an the base metric. In section IV we discuss our numerical simulations of interfaces on random cones, the critical exponents, and the radial fluctuations. The fact that all cones have TW-GUE radial fluctuations is justified in section V. Our conclusions and ideas for further work are finally outlined in section VI.

II. FROM THE COVARIANT KPZ EQUATION TO RANDOM METRICS

In previous works [14, 15], we have proposed an extension of the KPZ equation for which all terms are defined in a covariant manner, i.e., the equation has the same form when expressed on any background metric. The equation expresses the evolution of a closed simple curve representing an interface. Each point $\vec{r}$ on the curve moves along the local normal direction, with a velocity affected by three different terms:

$$\partial_t \vec{r} = [A_0 + A_1 k(\vec{r}) + A_n \eta(\vec{r})] \, \vec{n}(\vec{r}). \quad (1)$$

Here, $\vec{n}$ is the local unit normal vector, k is the geodesic curvature, and η is a zero-average Gaussian noise, uncorrelated both in time and along the interface. The con-

stants A_0, A_1, and A_n are free parameters, which characterize, respectively, irreversible growth, surface tension, and fluctuations in the growth events. In fact, this interface can develop self-intersections. Thus, Eq. (1) must be supplemented with an algorithm to treat them. A convenient choice is to remove always the smaller component [14, 15].

In [3] we focused on the simplest case of Eq. (1) with $A_1 = A_n = 0$, which we call the *Huygens equation*, namely,

$$\partial_t \vec{r} = \vec{n}(\vec{r}), \quad (2)$$

because it simply *propagates* any closed curve outwards, in a way which is similar to Huygens' principle for the propagation of a wavefront [16]. If our initial curve is an infinitesimal circumference around point X_0, then the evolution of our interface will be given by a set of *balls* on this metric, with linearly increasing radii. In [3] we applied Eq. (2) to the study of the growth of balls on two-dimensional *random* manifolds with smooth enough random metrics, which are flat on average and have short-range correlations.

In the present work we lift the condition that the random metrics need to be flat on average. Let us consider any background metric, given by the metric tensor field $g_0(x, y)$. We can introduce an ensemble of metrics through

$$g(x, y) = \nu(x, y) g_0(x, y), \quad (3)$$

where $\nu(x, y)$ is a smooth enough random field with uniform average and short-range correlations (as measured by the g_0 metric). This means that, at scales beyond the (small) correlation length of this random field ν, the metric $g_0(x, y)$ is subject to a random conformal transformation or, alternatively, that we consider an *optical metric* on the base manifold, with a position-dependent index of refraction.

III. CYLINDER, CONES, AND PLANE

Let us address the study of the statistical properties of interfaces generated by the Huygens equation (2) on random conformal deformations of a given base Riemannian manifold $g_0(x, y)$, as expressed by Eq. (3). The division of the KPZ class between band geometry and circular geometry can be recast in our Riemannian geometry language by stating that band geometry refers to propagation of Huygens equation on a cylinder, while circular geometry refers to propagation on a plane. Thus, for a random metric based on the plane, the results of [3] show that, as expected, the radial fluctuations obey TW-GUE statistics. On a random metric based on the cylinder, if we set up as initial condition a curve which wraps around it, the ensuing interface fluctuations should follow the TW-GOE distribution.
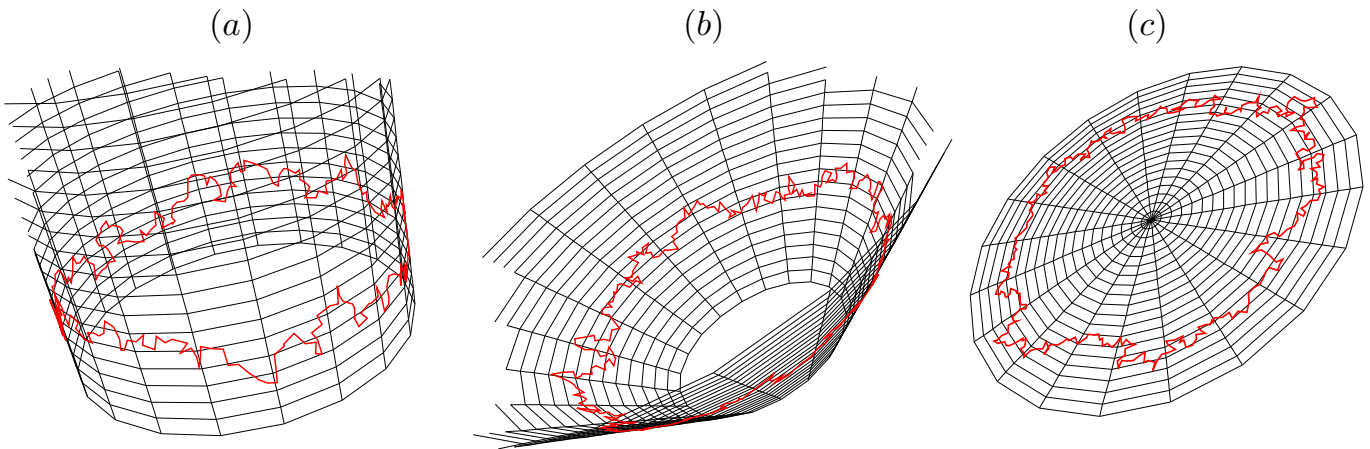
FIG. 1. Ball boundaries on a random manifold whose background metric is (a) a cylinder, (b) a cone, and (c) a plane. These interfaces have been generated using the numerical algorithm described in Sec. IV.

Let us define a natural family of surfaces which interpolates between the cylinder and the plane: a set of cones of increasing opening angle θ between the axis and the axis and the generatrix, with $\theta = 0$ for the cylinder and $\theta = \pi/2$ for the plane. See Fig. 2 for an illustration. The cone can be understood as a plane from which a wedge of angle $2\pi(1 - \sin\theta)$ has been removed. We will address the following question: how does the distribution for the normal fluctuations of the interface interpolate between TW-GOE for the random metric on the cylinder and TW-GUE for the random metric on the plane?

Cones are surfaces with zero Gaussian curvature K everywhere except at the vertex. The integral of K over any domain containing the vertex is always the same, and equal to the *angular defect* $\Delta = 2\pi(1 - \sin\theta)$ [19, 20]. The sum of the angles of any geodesic triangle containing the vertex will be $\pi + \Delta$. In fact, there is a stronger version of this statement, that is a consequence of the Gauss-Bonnet theorem:

$$\int_\gamma k_g \, ds = 2\pi \sin\theta. \tag{4}$$

Here, k_g is the geodesic curvature of any curve γ surrounding the vertex. In the case of a random metric based on the cone, Eq. (4) will be modified by fluctuations. Yet, it shows that the integral of the geodesic curvature is a conserved quantity on average, and we can expect some observables of our interfaces to depend on θ.

A. Coordinates and metric on the cones

Let us describe our cone manifolds in detail, starting with their embedding in 3D and moving to an intrinsic chart. Fig. 2 shows the surfaces embedded in 3D space, the (X, Y, Z) coordinates of an arbitrary point on one of
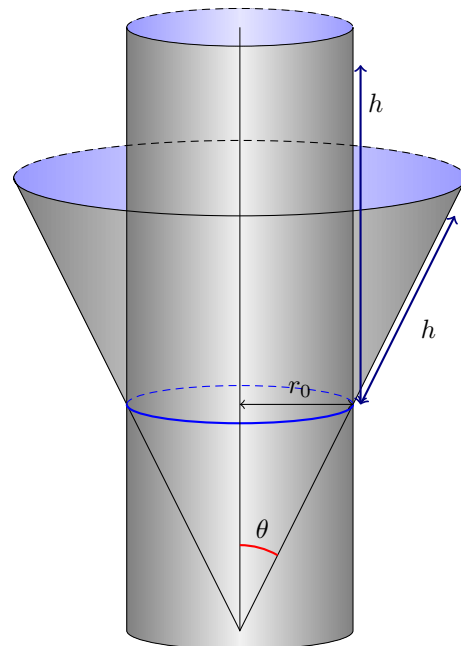

FIG. 2. Illustration for our family of conical surfaces, parametrized by θ, the angle between the cone axis and generatrix. They are all forced to coincide on a base circumference of radius r_0, marked with the blue line. Quasi-polar coordinates are defined by using a "radius" $r = r_0 + h$.

these surfaces being given by

$$X = (r_0 + h\sin\theta)\cos\phi, \tag{5a}$$
$$Y = (r_0 + h\sin\theta)\sin\phi, \tag{5b}$$
$$Z = h\cos\theta, \tag{5c}$$

where we have made the cones coincide on a base circumference of radius r_0 (the thick blue line in Fig. 2) for all θ, h is the distance of the point to the base circumference, and ϕ is the azimuthal angle. Let us choose a

quasi-polar coordinate chart on the cones, in which each point is given by the pair (r, ϕ), with $r = r_0 + h$. Thus, the base circumference will be described as $r = r_0$ on all the cones. This coordinate chart presents some advantages, such as an homogeneous description of all cones, cylinder, and plane. We can now consider the metric for the cones expressed on these coordinates,

$$ds^2 = dr^2 + \rho^2(r)d\phi^2, \tag{6}$$

where $\rho(r) = r_0 + h\sin\theta = r_0 + (r - r_0)\sin\theta$ is the distance to the axis of the cone. The limit case of the cylinder ($\theta = 0$) yields

$$ds^2 = dr^2 + r_0^2 d\phi^2. \tag{7}$$

Similarly, for the plane ($\theta = \pi/2$) we have

$$ds^2 = dr^2 + r^2 d\phi^2. \tag{8}$$

Despite the simplicity of this quasi-polar metric, we prefer to introduce a new Cartesian-like chart. The reason is to avoid the need for periodic boundary conditions in the azimuthal angle. Let us define x and y as

$$x = r\cos\phi, \tag{9a}$$
$$y = r\sin\phi. \tag{9b}$$

Geometrically, the Cartesian-like coordinates (x, y) express a mapping of the cone on the plane containing the base circumference, in which distances to this base curve are preserved. In these *quasi-Cartesian coordinates*, the metric can be written as

$$g_{xx} = \frac{2r_0 y^2 (r - r_0)\left(\sin\theta - \sin^2\theta\right) + r^4\sin^2\theta + \left(r_0^2 y^2 + r^2 x^2\right)\cos^2\theta}{r^4}, \tag{10a}$$

$$g_{yy} = \frac{2r_0 x^2 (r - r_0)\left(\sin\theta - \sin^2\theta\right) + r^4\sin^2\theta + \left(r_0^2 x^2 + r^2 y^2\right)\cos^2\theta}{r^4}, \tag{10b}$$

$$g_{xy} = g_{yx} = \frac{xy[\left(r^2 - r_0^2\right)\cos^2\theta - 2r_0 (r - r_0)\left(\sin\theta - \sin^2\theta\right)]}{r^4}. \tag{10c}$$

Our numerical simulations will be performed on the (x, y) plane, using the base metric described by Eq. (10).

IV.   NUMERICAL SIMULATIONS AND RESULTS

In this section we describe our numerical simulations of the evolution of the base circumference $x^2 + y^2 = r_0^2$ under Huygens equation (2), supplemented with the rule of self-intersection removal, on a random metric of the form (3), i.e., a random conformal perturbation of the metric g_0. In turn, g_0 will be one of our cone metrics, given by Eq. (6) in (quasi-)polar coordinates or by Eq. (10) in (quasi-)Cartesian coordinates.

We have extended the algorithm described in Ref. [3] in order to work on random conformal deformations of any given base Riemannian manifold. Let us summarize the algorithm. The interface is considered to be a piecewise linear simple curve, with an adaptive number of points: if two points separate beyond a certain threshold ℓ_{max} (in the base metric g_0), a new point is included mid-way [14]. In all cases, we take $\ell_{max} = 0.05$. Each segment of the interface determines a tangent vector $\vec{t}$ along the interface curve. We make it evolve along the local normal direction $\vec{n}$. In order to determine $\vec{n}$, we require the local metric tensor, $g(\vec{r})$. This is obtained, via Eq. (3),

by multiplying the local metric tensor of the base manifold by a random conformal factor, $\nu(\vec{r})$. Then, we solve the equation $\vec{t} \perp_g \vec{n}$, i.e., $g_{\mu\nu}(\vec{r})t^\mu n^\nu = 0$. The propagation of each segment at each time-step ($\Delta t = 0.005$) is performed in a straightforward way, but the evolution equation is supplemented with an algorithm in order to detect self-intersections [14]. As mentioned above, the smaller component is always removed so that the interface remains a simple curve at all times.

Figures 3 and 4 show some profiles obtained by our simulations, for a cylinder and for a cone with $\theta = \pi/4$, respectively. The initial radius is $r_0 = 15$ for the cylinder and $r_0 = 0.01$ for the cone. The local conformal factors $\nu(\vec{r})$ are uniform random deviates in $[1/20, 1]$ which are chosen independently at each point, since we assume our discretization cutoff ℓ_{max} to be larger than the correlation length for the ν field. In both figures, the top panel shows the ball profiles as obtained in the (x, y) coordinate chart. The top-right panel is a zoom of a single profile. The center panels show how the previous interfaces fit on the original manifolds, the cylinder and the cone. The bottom panel, in both cases, shows the interface evolved up to the same time, $t = 20$.
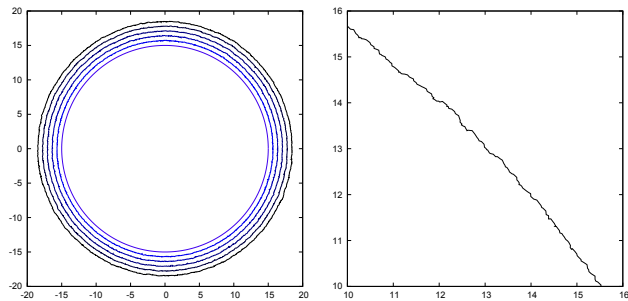
FIG. 3. Interfaces on a cylinder with $r_0 = 15$. Top panels: profiles in (x, y) coordinates. The top-right panel shows a zoom of the outermost profile in the top-left panel. Medium panel: profiles on the 3D cylinder. The simulation times are $t = 0$, 4, 8, 12, 16, and 20, bottom to top. Bottom panel: enlargement of the $t = 20$ profile shown in the center panel.

FIG. 4. Interfaces on a cone with $\theta = \pi/4$ and $r_0 = 0.01$. Top panels: profiles in (x, y) coordinates. The top-right panel shows a zoom of the outermost profile in the top-left panel. Medium panel: profiles on the 3D cylinder. The simulation times are $t = 0$, 4, 8, 12, 16, and 20, bottom to top. Bottom panel: enlargement of the $t = 20$ profile shown in the center panel.

A. Critical exponents

As described in Ref. [3], ball boundaries on a flat-average random metric of the form of Eq. (3) follow the Family-Vicsek Ansatz when considered as interfaces. Specifically, the roughness of the ball boundary, as measured in the Euclidean metric, grows with time as a power-law, $W(t) \sim t^\beta$, and so does the correlation length along the interface, $\xi(t) \sim t^{1/z}$. Moreover, in the case studied in [3], the values of the critical exponents were
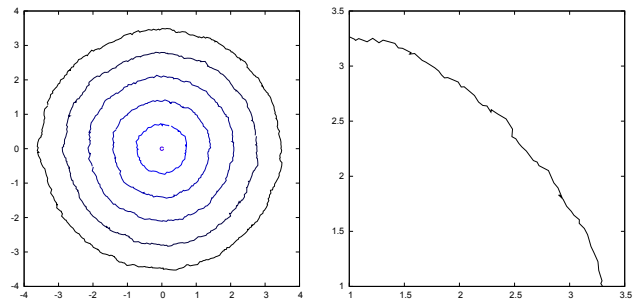
shown to be those of the Kardar-Parisi-Zhang universality class, $\beta = 1/3$ and $1/z = 2/3$.

Let us now consider the interfaces produced by Huygens equation (2) on our random cones. The average shape of the ball boundary for any given time is expected to be a circumference of radius proportional to t. Although we do not have a proper shape theorem for our general case, see [21, 22] for some rigorous shape theorems in particular manifolds. We define the roughness of
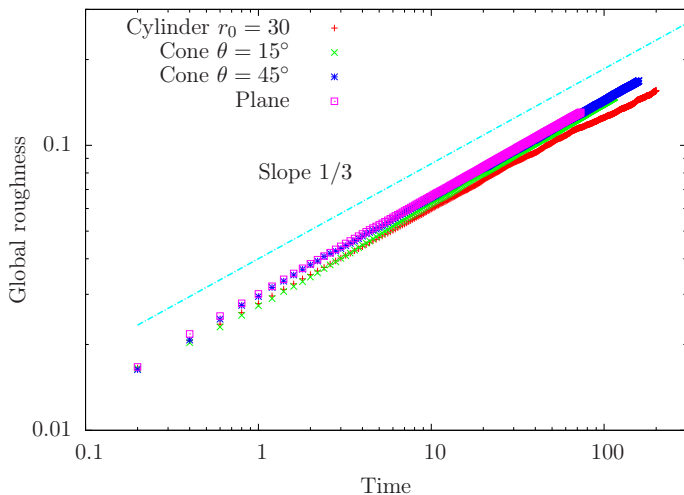
FIG. 5. Average roughness W as a function of time for interfaces grown with Huygens equation (2) on conformal random deformations of metrics corresponding to a cylinder of radius $r_0 = 30$, cones with opening angles $\theta = 15°$ and $45°$, and a plane. In all cases, the roughness exponent is close to $1/3$.

a curve W as the expected magnitude of the normal deviations of the actual interface from its best-fit circumference centered at the origin. Notice that distances along the radial direction in the (x, y) chart can be computed in an Euclidean setting. Fig. 5 shows these measurements of W as a function of time, averaged over 100 realizations of the disorder, for a cylinder of radius $r_0 = 30$, a cone with opening angle $\theta = 15°$ and $r_0 = 0.1$, another cone with $45°$ and $r_0 = 0.01$, and the plane. In all cases, the power-law behavior of the roughness with time, $W \sim t^\beta$, is clear-cut, with a value of β which is very close to $1/3$, as expected. Note, among all cases, the cylinder is the only one for which roughness saturation at long times to a system-size dependent value may influence the measured value of β. In view of the fact that higher-order cumulants do not seem to change trend for our simulations of the cylinder case (see next section), we believe our simulation times are not significantly affected by saturation effects in this case.

The Family-Vicsek Ansatz also implies that the average roughness on windows of size ℓ will scale as $w(\ell) \sim \ell^\alpha$ if ℓ is smaller than the surface correlation length, $\xi(t)$. Moreover, the three critical exponents are related via $\alpha/\beta = z$. In our case, direct measurements of the roughness exponent α are involved, because distances along the curve should be carefully computed. In order to overcome this difficulty, we have devised a novel technique to measure the correlation length, which is illustrated in Fig. 6. For a given interface, we draw the best-fit circumference with center at the origin, and mark all the intersection points between the circumference and the actual interface. They divide the circumference into a series of n patches or arcs, whose actual lengths $\{\ell_1, \ell_2, \cdots, \ell_n\}$ on the cone are measured along the azimuthal direction, being given by
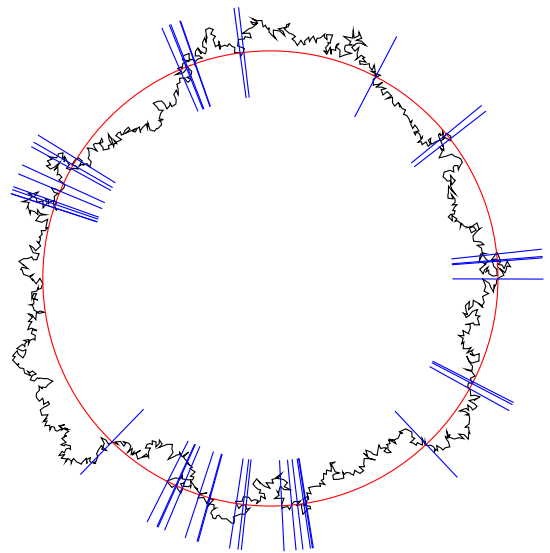

FIG. 6. Illustration of the procedure to estimate the surface correlation length $\xi(t)$. The profile is superimposed onto the best-fit circumference centered at the origin, and the intersection points are marked. The correlation length is estimated as the expected length of the patch to which a random point on the circumference belongs.

$$\ell_i = \Delta\phi_i \left(r_0 + (\bar{r} - r_0) \sin\theta \right), \qquad (11)$$

where $\bar{r}$ is the radius of the best-fit circumference.

We can estimate the correlation length asking the following question: if we choose a random point on the circumference, what is the expected length of the patch on which it stands? On average, this value will be given by

$$\xi \equiv \frac{\sum_i \ell_i^2}{\sum_i \ell_i}. \qquad (12)$$

Notice that this value does not correspond to the average value for the patch lengths. The behavior of this correlation length ξ is shown in Fig. 7, where we can see that it follows a power-law, with exponent close to the KPZ value $1/z = 2/3$ in all cases. Thus, we have checked the first claim, that the interfaces on cylinder, cones and plane, in all cases show the critical exponents of the KPZ universality class.

B. Radial Fluctuations

The KPZ universality class does not only entail the values of the critical exponents. As discussed above, the radial fluctuations are expected to follow one of the well known Tracy-Widom probability distributions. In
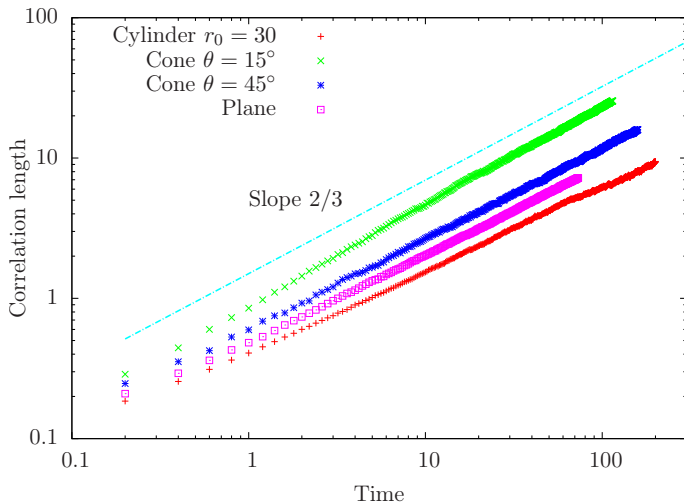
FIG. 7. Growth of the correlation length $\xi(t)$ for interfaces of different geometries: cylinder of radius $r_0 = 30$, cones with angles $\theta = 15°$ and $45°$, and a plane. In all cases $\xi(t) \sim t^{1/z}$ with $1/z$ very close to $2/3$.

the case of a ball on a random metric over the plane, it was shown in Ref. [3] that they indeed follow the Tracy-Widom statistics for the Gaussian unitary ensemble (TW-GUE).

We have developed an extension of the analysis in [3] in order to obtain the radial fluctuations histogram for interfaces following the Huygens equation (2) on random conformal deformations of a base Riemannian manifold, Eq. (3), assuming that a growing circumference is a solution of the aforementioned Eq. (2). Along the simulation procedure described at the beginning of this section, the radial data are stored along with their time tag. We consider all pairs (t_i, r_i), from different noise realizations and times, and fit them to a linear form $r_i = \varrho + v t_i$, whereby constant values ϱ and v are obtained. Then, we fit the remainders to a power law with time, namely,

$$(r_i - (\varrho + v t_i))^2 = \Gamma^2 t^{2\beta}. \tag{13}$$

Using the ensuing values of Γ and β (=1/3), we finally extract the rescaled radial fluctuation χ as

$$\chi_i \equiv \frac{r_i - (\varrho + v t_i)}{\Gamma t_i^\beta}. \tag{14}$$

Notice that, by construction, this χ variable has zero mean and unit variance, and that it is invariant under affine changes in the radii r. We then proceed to obtain the histogram for these $\{\chi_i\}$. The theoretical prediction is that these histograms will correspond to the (suitably normailzed) TW-GOE and TW-GUE distributions in the extremes of our family of surfaces: TW-GOE for the cylinder ($\theta = 0$) [3] and TW-GUE for the plane ($\theta = \pi/2$). In order to assess the statistics of interface

fluctuations, note that one could alternatively [? ?] measure Γ and ϱ from suitable moments of the interface radial positions and compare the histograms of the ensuing stochastic variable to the suitable standard TW distribution (with non-zero average and universal variance).

Let us remark that the values of Γ that we obtain following the procedure in [3] as indicated above are the same for all the cones within our numerical accuracy, $\Gamma = 0.03(2)$ in all cases, as expected from the theoretical results in [25]. This result could have been anticipated from Fig. 5, where all the roughness curves can be seen to (nearly) collapse. Moreover, the sign of the effective growth parameter (usually known as λ) is positive, the same as in systems with a net radial growth velocity [3].

These measurements have been carried out in three cases: (A) a cylinder with $r_0 = 15$, for which we run 500 noise realizations and gather all the points obtained from 1000 snapshots in the time interval $t \in [1, 10]$ for each noise configuration, giving a total of $7 \cdot 10^7$ points; (B) a cone with $\theta = 15°$, $r_0 = 0.1$, 500 realizations and 500 snapshots for each one with $t \in [100, 200]$, a total of $3 \cdot 10^7$ points; (C) a cone with $\theta = 45°$, 100 realizations and 1000 snapshots for each one with $t \in [10, 80]$, a total of $4 \cdot 10^8$ points; (D) a plane, $\theta = 90°$, with 500 realizations in $t \in [10, 27]$.

Before giving a quantitative assessment, let us consider the visualization of these results as shown in Fig. 8. Since the TW-GUE and TW-GOE distributions are very close visually to the normal distribution, we plot the difference with the normalized Gaussian probability density function, $\rho(\chi) = (2\pi)^{-1/2} \exp(-\chi^2/2)$, which we call here *non-Gaussianity*. The top panel shows the non-Gaussianity as a function of χ for the exact TW-GOE and TW-GUE distributions, and for the obtained radial fluctuations on the cylinder with $r_0 = 15$, which fit closely the TW-GOE distribution, as expected. The central and bottom panels show the analogous data for the cone with $\theta = 15°$ (central panel) and $\theta = 45°$ (bottom panel). In these two cases, the empirical distribution fits closely the TW-GUE distribution, as we know to be the case for the plane [3]. But, of course, this check is merely visual, and should be supplemented with further numerical comparisons.

A more strict test is provided by the estimation of the third and fourth cumulants of the distributions, normalized as the skewness and the kurtosis, as shown in Table I. The data for the cylinder can be seeen to correspond approximately to the TW-GOE distribution, while they fit the TW-GUE distribution for the cones in all cases. Fig. 9 shows the time evolution of the skewness of the distribution, convoluted with a Gaussian filter with deviation $\sigma = 5$ in order to highlight the trends of the various sets of data. We can see that, for all the cones and the plane, the skewness values converge slowly towards the TW-GUE value, while for the cylinder it fluctuates around the TW-GOE one.
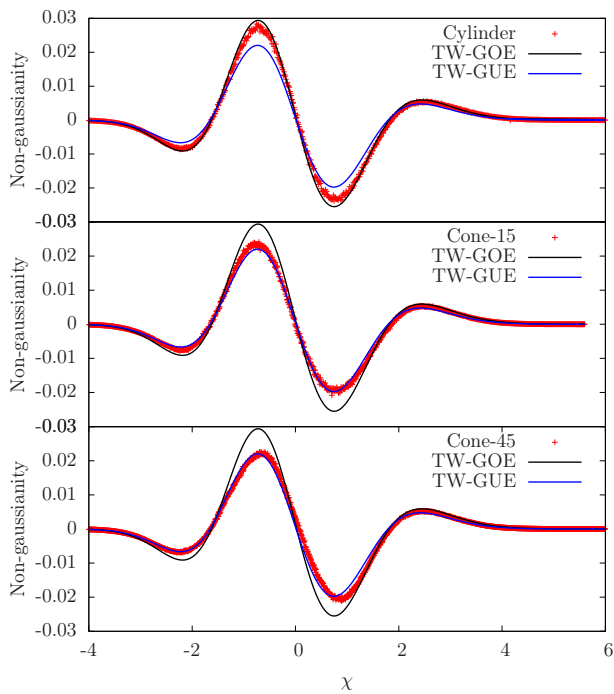
Another interesting measure is provided by the

FIG. 8. Difference with a Gaussian (non-Gaussianity) of the radial fluctuations of interfaces grown with Huygens Eq. (2) on random conformal deformations of our base manifolds: top, cylinder with $r_0 = 15$; center: cone with $\theta = 15°$; bottom: cone with $\theta = 45°$. Each panel includes the non-Gaussianity of the TW-GOE and TW-GUE distributions, for easy comparison. Notice that the cylinder corresponds to TW-GOE statistics, as expected, while the cones follow TW-GUE statistics. Further numerical checks are discussed in the text.

	Skewness	Kurtosis
TW-GOE	0.2934	0.1652
TW-GUE	0.2241	0.0934
Cylinder $r_0 = 15$	0.30	0.18
Cone ($\theta = 15°$)	0.24	0.10
Cone ($\theta = 45°$)	0.23	0.13
Plane	0.22	0.10

TABLE I. Skewness and kurtosis of the radial scaled variable χ, Eq. (14), for different base manifolds, as compared to the exact TW values.

Kullback-Leibler (KL) divergence between the empirical histograms and the theoretical distributions. The KL divergence $D(P||Q)$ between two probability distributions P and Q is defined as the loss of information when data samples from P are assumed to stem from Q [26], and can be regarded as a natural distance in the space of distributions. It can be computed as

$$D(P||Q) = \int \mu_P \log\left(\frac{P}{Q}\right), \qquad (15)$$

where μ_P is the measure induced by distribution P. Table II shows the KL divergences between the empirical
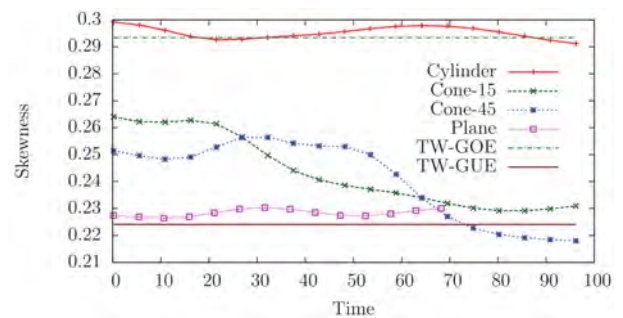

FIG. 9. Time evolution of the skewness of the radial distribution for the cylinder, cones, and plane, along with the values for TW-GUE and TW-GOE, convoluted with a Gaussian filter with deviation $\sigma = 5$ in order to highlight the trends. Notice that, for long times, the cylinder fluctuates around the TW-GOE value, while for all cones and the plane the skewness approaches the TW-GUE value. Notice that the initial radius r_0 is different for the 15° cone and for the 45° one.

χ distributions and the TW-GUE and TW-GOE distributions. It can be seen that, on the cylinder, the radial fluctuations are more likely TW-GOE, but on all cones the radial fluctuations are closer to TW-GUE.

KL-Distance to:	TW-GOE	TW-GUE
Cylinder $r_0 = 15$	$2.7 \cdot 10^{-5}$	$2.5 \cdot 10^{-4}$
Cone ($\theta = 15°$)	$2.9 \cdot 10^{-4}$	$8.3 \cdot 10^{-5}$
Cone ($\theta = 45°$)	$5.2 \cdot 10^{-4}$	$2.6 \cdot 10^{-4}$
Plane	$5.2 \cdot 10^{-4}$	$1.3 \cdot 10^{-4}$

TABLE II. Kullback-Leibler (KL) divergences, Eq. (15), between the empirical χ distributions and the theoretical TW-GOE and TW-GUE distributions.

V. GROWTH, GEOMETRY, AND TOPOLOGY

The numerical simulations discussed in the previous section allow us to extract several hypothesis. First, Huygens propagation on random conformal deformations of cones of different opening angles are shown to fall into the KPZ universality class, for all opening angles. We can also conjecture that, on the cylinder, the radial fluctuations follow TW-GOE statistics, while for all the cones with $\theta > 0$ we obtain TW-GUE. This conjecture fits well with the results of [12, 13], where it was shown that growth in a band geometry whose substrate expands at a constant rate in time follows the TW-GUE distribution. In our geometric setting, an expanding substrate is similar to a cylinder with a growing radius, i.e., a cone.

These results require some theoretical explanation, which we will attempt within our Riemannian geometry framework. Let us recall that Huygens equation (2) is *covariant*: solutions obtained using one coordinate chart can be mapped into solutions obtained using a different

coordinate chart. The base metric tensor for all our surfaces, in a polar chart (r, ϕ), has the form

$$g(r, \phi) = \begin{pmatrix} 1 & 0 \\ 0 & f(r) \end{pmatrix}, \tag{16}$$

where $f(r) = (r_0 + (r - r_0) \sin \theta)^2$. If $\theta \neq 0$, an affine change of coordinates,

$$r \to \quad \hat{r} = r - r_0 + \frac{r_0}{\sin \theta}, \tag{17}$$

$$\phi \to \quad \hat{\phi} = \phi \sin \theta, \tag{18}$$

renders the metric Euclidean. Notice that this corresponds to viewing the cone as a plane from which a wedge of angle $2\pi(1 - \sin \theta)$ has been removed. For $\theta = 0$, of course, the change of variables (18) becomes singular. And, as noted in the previous section, an affine transformation in the r coordinate will *not change the χ distribution.*

Let us now turn our attention to the conformal noise imposed upon the base metric. Since we assume it to be uncorrelated in space, we can safely assume that it will be invariant under coordinate changes. Combining both statements we find that, if $\theta \neq 0$, *the radial fluctuations for growth of any cone must have the same form as in the Euclidean case.* The same argument can not be applied to growth on the cylinder, since in that case the metric factor $f_{cyl}(r) = r_0$, and no affine change of coordinates in r will map it to the Euclidean case $f_{Euc}(r) = r$. Notwithstanding, please notice that our argument does not entail that the cylinder and the plane must have different fluctuations.

Despite the metric nature of our argument, the difference between the cylinder and the rest of the cones is, moreover, topological. All cones are homeomorphic to the plane, while the cylinder is not. In fact, on the cylinder the Huygens equation is applied in a different way. For any cone, we can start with an infinitesimal circumference around the vertex and produce balls around it. In the cylinder, we must start with a curve which is not homotopically equivalent to a point, because it will wrap around the manifold. But this difference by itself does not allow us to assert that growth on the cylinder will possess different kinds of fluctuations, since the cylinder can be smoothly *completed* with a lower lid, thus rendering our initial circumference homotopically trivial. Thus, the difference between TW-GUE and TW-GOE behavior does not stem from the homotopy class of the initial curve.

VI. CONCLUSIONS AND OUTLOOK

We have investigated the universality subclass structure of the KPZ class in a Riemannian geometry setting for disordered substrates. We have studied the statistical properties of *Huygens* interfaces on random metrics, see Eq. (2). A Huygens interface is defined as a the propagation of an initial simple closed curve on a certain manifold, always following the local normal direction with unit speed. The metrics studied were conformal random deformations of a certain set of base manifolds: the Euclidean plane, cones of different opening angles, and a cylinder. Note, in all these systems disorder is quenched. Nontheless, fluctuations of ball interfaces are in the KPZ universality class associated with time-dependent noise. Indeed, while in the planar case it had already been shown [3] that the interfaces follow KPZ statistics with TW-GUE radial fluctuations, in the present work we have shown how KPZ statistics are found in all other manifolds, with TW-GUE fluctuations for the cones and TW-GOE for the cylinder. There is no intermediate subclass between these two.

A theoretical explanation of this result has been put forward, based on the notion that the Huygens equation is *covariant*, i.e., it can be studied in any possible coordinate chart. All cones with non-zero opening angle are homeomorphic to the Euclidean plane, but not to the cylinder. Moreover, we have written down the explicit non-singular change of coordinates between the cones and the plane and shown that it has no effect on the statistical properties of the radial fluctuations of the interfaces, implying that all cones should present TW-GUE statistics. This result fits very well with the results of [12, 13], where it was shown that KPZ systems (a discrete model and the KPZ equation itself) in band geometry with an expanding substrate also feature TW-GUE statistics.

Another relevant conclusion for our work that remains beyond the approaches in [12, 13] is that growing interfaces with global curvature may still present TW-GOE fluctuations, as shown in our rendering of the solutions of the Huygens equation on the randomized cylinder. One may argue that the global curvature of these interfaces is merely apparent, because their integrated geodesic curvature is, indeed, zero. This points to the need of a deeper geometric understanding of the KPZ subclass structure within the Riemannian geometry framework.

Regarding technical aspects, we have introduced a novel way to estimate the correlation length of the interface, by considering the expected value of the distance between intersections with the average circumference, see Fig. 6. Moreover, we have employed techniques from information theory in order to determine the probability distribution, such as the Kullback-Leibler divergence, see Eq. 15.

Our work opens up many possibilities: what are the statistical properties of the covariant KPZ equation on a generic manifold? Or, alternatively, which are the statistics of the Huygens equation on random deformations of a certain base manifold? In this case, we expect a far richer set of possibilities. The argument described in Sec. V suggests a possible methodology in order to extract the radial fluctuations when the manifold is homeomorphic

to either the cylinder or the plane. But it leaves open the question regarding additional flavors or subclasses of the celebrated KPZ universality class.

Another relevant question is whether this strategy to characterize subclasses within the KPZ universality class will extend to higher dimensions, and whether they will be related to topological considerations, as suggested by recent work on directed polymers in random media (DPRM) in 2+1D [27, 28]. A comparison of the Huygens and the DPRM methods is in order, which may lead to very interesting results.

[1] A.-L. Barabási and H.E. Stanley, *Fractal Concepts in Surface Growth*, Cambridge University Press (1995).

[2] M. Kardar, G. Parisi, and Y.-C. Zhang, Phys. Rev. Lett. **56**, 889 (1986).

[3] S.N. Santalla, J. Rodriguez-Laguna, T. LaGatta, and R. Cuerno, New J. Phys. **17**, 033018 (2015).

[4] M. Prähofer and H. Spohn, Phys. Rev. Lett. **84**, 4882 (2000).

[5] K.A. Takeuchi and M. Sano, Phys. Rev. Lett. **104**, 230601 (2010).

[6] T. Sasamoto and H. Spohn, Phys. Rev. Lett. **104**, 230602 (2010).

[7] G. Amir, I. Corwin, and J. Quastel, Comm. Pure Appl. Math. **64**, 466 (2011).

[8] I. Corwin, Random Matrices: Theory and Appl. **1**, 1130001 (2012).

[9] P. Calabrese, P. Le Doussal, Phys. Rev. Lett. **106**, 250603 (2011); P. Le Doussal, P. Calabrese, J. Stat. Mech. P06001 (2012).

[10] S. Prolhac, Phys. Rev. Lett. **116**, 090601 (2016).

[11] J. Baik and Z. Liu, arXiv:1605.07102[math-ph] (2016).

[12] S.S. Carrasco, K.A. Takeuchi, S.C. Ferreira, and T.J. Oliveira, New J. Phys. **16**, 123057 (2014).

[13] T. Halpin-Healy and K.A. Takeuchi, J. Stat. Phys. **160**, 794 (2015).

[14] J. Rodriguez-Laguna, S.N. Santalla, and R. Cuerno, J. Stat. Mech.: Theory Exp. **2011**, P05032 (2011).

[15] S.N. Santalla, J. Rodriguez-Laguna, and R. Cuerno, Phys. Rev. E **89**, 010401(R) (2014).

[16] J.A. Sethian, *Level Set Methods and Fast Marching Methods*, Cambridge University Press (2005).

[17] A. Borodin, P. L. Ferrari, and T. Sasamoto, Commun. Pure Appl. Math. **61**, 1603 (2008).

[18] P. Le Doussal, J. Stat. Mech.: Theory Exp. **2014**, P04018 (2014).

[19] I.M. Singer and J.A. Thorpe, *Lectures notes on elementary topology and geometry*, Springer (1976).

[20] S.L. Devadoss and J. O'Rourke, *Discrete and computational geometry*, Princeton University Press (2011).

[21] H. Kesten and V. Sidoravicius, Ann. Math. **167**, 701 (2008).

[22] T. LaGatta and J. Wehr, J. Math. Phys. **51**, 053502 (2010).

[23] S. G. Alves, T. J. Oliveira, S. C. Ferreira, Europhys. Lett. **96**, 48003 (2011).

[24] T. J. Oliveira, S. C. Ferreira, and S. G. Alves, Phys. Rev. E **85**, 010601(R) (2012).

[25] J. Krug, P. Meakin, and T. Halpin-Healy, Phys. Rev. A **45**, 638 (1992).

[26] E. Desurvire, *Classical and quantum information theory*, Cambridge University Press (2009).

[27] T. Halpin-Healy, Phys. Rev. Lett. **109**, 170602 (2012).

[28] T. Halpin-Healy, Phys. Rev. E **88**, 042118 (2013).